The unique procoagulant adaptations of pseudonaja textilis venom factor V and factor X

Schreuder, M.

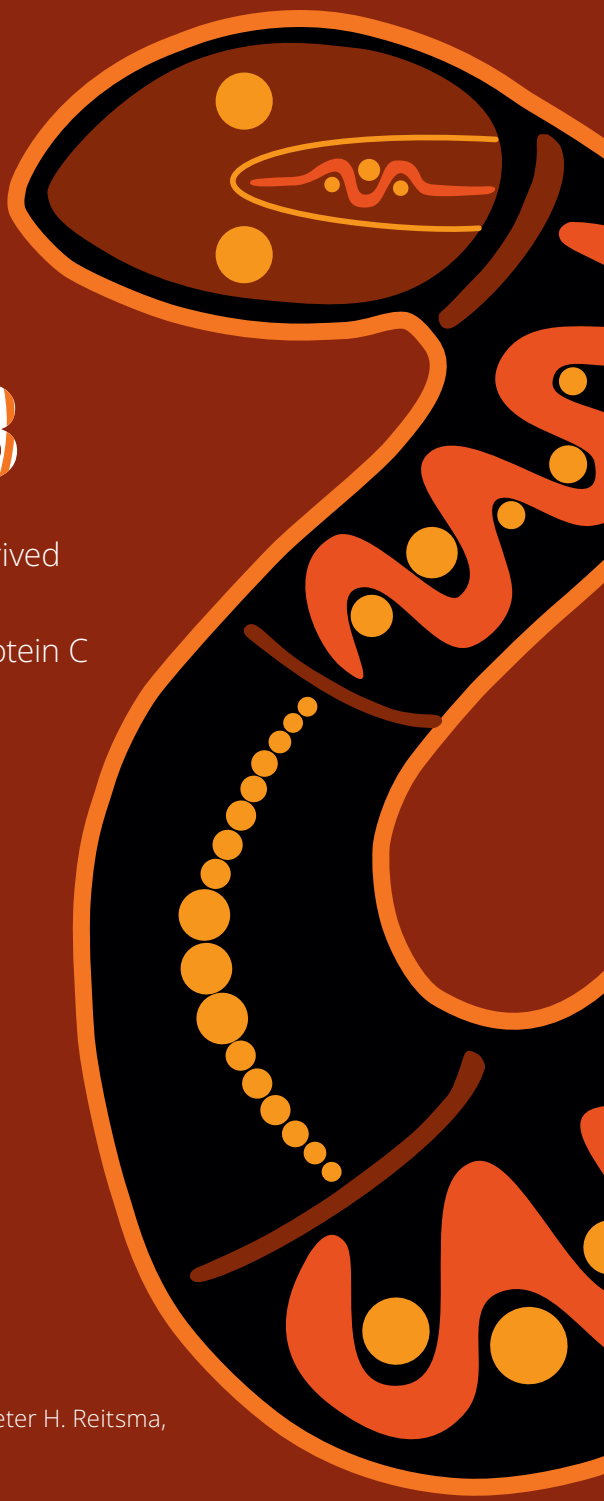

Chapter 3

ptFVa (*Pseudonaja Textilis* Venom-Derived Factor Va) Retains Structural Integrity Following Proteolysis by Activated Protein C

Mark Schreuder, Xiaosong Liu, Ka Lei Cheung, Pieter H. Reitsma, Gerry A.F. Nicolaes, Mettine H.A. Bos

Accepted in Arteriosclerosis, Thrombosis, and Vascular Biology.

Abstract

Objective: The Australian snake venom ptFV (*Pseudonaja textilis* venom-derived factor V) variant retains cofactor function despite APC (activated protein C)-dependent proteolysis. Here, we aimed to unravel the mechanistic principles by determining the role of the absent Arg306 cleavage site that is required for the inactivation of FVa (mammalian factor Va).

Approach and Results: Our findings show that in contrast to human FVa, APC-catalyzed proteolysis of ptFVa at Arg306 and Lys507 does not abrogate ptFVa cofactor function. Remarkably, the structural integrity of APC-proteolyzed ptFVa is maintained indicating that stable non-covalent interactions prevent A2-domain dissociation. Using Molecular Dynamics simulations, we uncovered key regions located in the A1 and A2 domain that may be at the basis of this remarkable characteristic.

Conclusions: Taken together, we report a completely novel role for uniquely adapted regions in ptFVa that prevent A2 domain dissociation. As such, these results challenge our current understanding by which strict regulatory mechanisms control FVa activity.

Introduction

Blood coagulation is a tightly regulated process composed of the sequential and concerted action of several serine proteases and their respective cofactors, together responsible for minimizing blood loss following vascular injury. Central to this process is the activation of coagulation factor V (FV) into the active cofactor Va (FVa)[1-3]. Once FV is partially or fully activated, it functions as cofactor for the serine protease factor Xa (FXa) by formation of the prothrombinase complex on the surface of an anionic membrane in the presence of calcium ions[4,5]. This complex rapidly converts prothrombin to thrombin, a key regulatory enzyme in coagulation. The coagulation system can also be exploited to gain selective advantages. The procoagulant venom of several Australian Elapid snakes contains a powerful enzyme complex that specifically activates prothrombin to disrupt the prey's intrinsic hemostatic balance[6-9]. This prothrombin-activating complex consists of FX- and FV-like proteins[10-13] comprising certain remarkable gain-of-function adaptations that enable this prothrombinase-like complex to initiate coagulation in an uncontrolled manner[14-17]. Rao *et al*[11] and our group[14,18] have demonstrated that venom FV derived from the common brown snake *Pseudonaja textilis* (ptFV), while undergoing selective proteolysis, is functionally resistant to FVa's natural inhibitor activated protein C (APC).

To downregulate the procoagulant response, coagulant FVa is inactivated by APC via proteolysis of the A2 domain residues Arg306, Arg506, and Arg679[19-23]. Cleavage at Arg306 and Arg506 results in A2 domain dissociation and subsequent loss of FXa affinity[24]. While ptFVa is cleaved at a position that is homologous to human Arg506 (Lys507)[14], an Arg306-like cleavage site is absent[11,14]. Furthermore, venom FV comprises a unique disulfide bond that covalently links the A2 and A3 domains[14,16]. Although we have previously reported that this disulfide bond is not responsible for the functional APC resistance[18], whether it might stabilize the A2 domain binding affinity upon introduction of the Arg306 cleavage site remains to be determined.

In the present study, we generated several chimeric ptFV variants with the goal of uncovering the mechanistic principles of its exceptional functional resistance to APC. Our results demonstrate that ptFV has uniquely adapted several structural elements to prevent A2 domain dissociation and ptFVa inactivation. As such, these findings highlight the remarkable evolutionary adaptations that have made ptFVa into an extremely stable procoagulant venom and provide new insights in the structural requirements of APC-induced FVa inactivation.

Materials and Methods

Materials and Reagents: The inhibitor dansylarginine-N-(3-ethyl-1,5-pentanediyl)amide (DAPA) was from Haematologic Technologies (Essex Junction, VT). The peptidyl substrate H-D-Phe-Pip-Arg-pNA (S2238) was obtained from Instrumentation Laboratories (Bedford, MA, USA). All tissue culture reagents were from Life Technologies (Carlsbad, CA, USA). Small unilamellar phospholipid vesicles (PCPS) composed of 75% (wt/wt) hen egg L-phosphatidylcholine (PC) and 25% (wt/wt) porcine brain L-phosphatidylserine (PS) (Avanti Polar Lipids, Alabaster, AL, USA) were prepared and characterized as described previously[25]. FV-depleted human plasma and Neoplastine CI Plus 10 prothrombin time (PT) reagent were obtained from Diagnostica Stago (Paris, France). All functional assays were performed in HEPES buffered saline (HBS: 20 mM HEPES, 0.15 M NaCl, pH 7.5) supplemented with 5 mM $CaCl_2$, 0.1% PEG8000 and filtered over a 0.2 µm filter (assay buffer).

Proteins: The human plasma-derived coagulation factors FXa, prothrombin, α-thrombin, APC, protein S, and plasmin were from Haematologic Technologies (Essex Junction, VT). Restriction endonucleases XcmI and Bsu36I were obtained from New England Biolabs (Ipswich, MA, USA). Recombinant venom-derived *Pseudonaja textilis* FXa (ptFXa) was prepared, purified, and characterized as described[18]. Recombinant constitutively active B-domainless human factor V (FV-810; hFV) and venom-derived ptFV were prepared, purified, and characterized as described previously[14,26]. The molecular weight and the extinction coefficients ($E_{0.1\%,\ 280\ nm}$) of the newly generated hFV-pt306, ptFV-h306, and ptFV-h306 S-S were assumed to be equal to hFV (216,000 kDa; 1.54) and ptFV (163,000 kDa; 1.25), respectively[14,26].

Construction of FV Variants: Constructs encoding for hFV comprising the ptFV Arg306 region (ptFV sequence Gly303-Thr309; Uniprot: Q7SZN0), designated pED-hFV-pt306, and ptFV comprising the human Arg306 region sequence (human full-length FV sequence Pro302-Leu308; Uniprot: P12259), named pED-ptFV-h306 were generated. Subsequently, ptFV's unique disulfide bond (ptFV residues Cys642 and Cys1002[16]; Uniprot: Q7SZN0) was removed by replacing the cysteines for serine residues, thereby creating pED-ptFV-h306 S-S. ptFV-h306 and ptFV-h306 S-S were generated employing mutagenic complementary oligonucleotides as described[14]. The variant hFV-pt306 was generated using a pUC57 plasmid encoding pED-ptFV nucleotides 2124-2144, flanked by pED-hFV nucleotides, which was generated and purchased from Genscript (Piscataway, NJ, USA). The resulting pUC57 plasmid was digested with XcmI and Bsu36I, gel-purified, and subcloned into pED-hFV via digestion with the same enzymes.

Expression and Purification of FV variants: Transfection of the plasmids encoding FV variants into baby hamster kidney cells, the selection of stable clones, and the expression and purification of hFV and ptFV were performed as described previously [14,26]. Briefly, FV proteins were purified employing ion-exchange chromatography on a Q-Sepharose FF (hFV variants) or SP-Sepharose (ptFV variants) column (GE Healthcare) using a NaCl elution gradient in HBS supplemented with 5 mM $CaCl_2$ and 1 mM benzamidine (BZA), pH 7.4. Fractions containing FV activity were pooled and dialyzed against 20 mM HEPES, 5mM $CaCl_2$, pH 7.4 for human FV variants or 20 mM MES, 5 mM $CaCl_2$, pH 6.0 for ptFV variants, loaded on a POROS HQ/20 (hFV variants) or HS/20 column (ptFV variants) (Applied Biosystems) and eluted using a NaCl gradient. Protein purity was assessed by SDS-PAGE analysis using pre-cast 4%–12% gradient gels under nonreducing and reducing conditions (50mM DTT) using the MOPS buffer system (Life technologies; Carlsbad, CA, USA) followed by staining with Coomassie Brilliant Blue R-250. For pretreatment with thrombin, FV variants were incubated for 15 minutes with α-thrombin (molar ratio: hFV 15:1; ptFV 3.75:1) in assay buffer at 37°C, followed by the addition of a 10-fold molar excess of hirudin over thrombin.

Factor Va-dependent Prothrombin Activation: Steady-state initial velocities of macromolecular substrate cleavage were determined discontinuously at 25 °C in assay buffer as described[27,28]. Briefly, unless otherwise stated, progress curves of prothrombin were obtained by incubating PCPS (50 μM), DAPA (10 μM), and prothrombin (1.4 μM) with the various recombinant FV(a) species (0-40 nM), and the reaction was initiated with 0.4 nM of FXa or ptFXa upon which the rate of prothrombin conversion was measured[27].

Activated Protein C-mediated Inactivation of FVa variants: For APC-mediated proteolysis, FVa variants (500 nM) were first incubated at 37 °C with APC (hFVa 10 nM; ptFVa 750 nM) in the presence of PCPS (50 μM). In addition, similar reactions containing ptFVa variants (50 nM) and PCPS (50 μM) were treated with 75 nM APC in the presence of protein S (100nM). Following APC-treatment, aliquots were taken and assayed for cofactor activity. Activity assay mixtures contained prothrombin (1.4 μM), PCPS (50 μM), DAPA (10 μM), APC-proteolyzed hFVa (0.2 nM) or ptFVa variants (0.1 nM), and FXa (2 nM) or ptFXa (1 nM), respectively. Prothrombin activation was determined as described[27]. Identification of the APC cleavage sites by N-terminal sequence analysis was performed at The Protein Facility of the Iowa State University Office of Biotechnology (Ames, IA).

Size-exclusion Chromatography of Activated Protein C-treated FVa Variants: FVa variants (100-500 μg) were subjected to APC treatment (hFVa 154.2 nM; ptFVa 1000 nM) for 15 (hFVa) or 180 min (ptFVa) at 37 °C in the presence of 50 μM PCPS. Reactions were quenched by the addition of 50 μM PPACK and 1 mM BZA. A 10 mm × 300 mm column

containing Superdex 200 Increase (GE Healthcare) was equilibrated in assay buffer supplemented with 50 µM PPACK and 1 mM BZA. The 100-400 µL reaction mixture was then applied to the column and eluted with equilibration buffer at a flow rate of 0.25 mL min^{-1} at room temperature. Fractions (0.25 mL) were collected and analyzed by SDS-PAGE or Western Blot using a polyclonal antibody directed against human FV (Affinity biologicals, Ancaster, Canada) and the monoclonal antibody directed against the Asn307-Arg506 fragment (AHV-5146; Haematologic Technologies, Essex Junction, VT) as described[29].

Molecular Structure Preparation: For molecular dynamics (MD) simulation[30], the 3D structures of hFVa[31] and ptFV (PDB ID: 4BXS) were used to build in missing loops with Loop Modeling suite in YASARA[32]. In addition, to simulate the experimentally used ptFV variant, the original region (303-GNPDTLT-309) was exchanged for the human Arg306 region (302-PKKTRNL-308), and the unique Cys642-Cys1002 disulfide bond was disrupted. To mimic the APC-cleaved protein structure, both human and *P. textilis* FV were separated into two protein fragments, reflecting their state after cleavage by APC at Arg306 and Arg506/Lys507. To expedite simulations, the C1 and C2 domain structures were excluded from simulation for both the human and *P. textilis* FV structures, given that these domains are structurally non-related with the A2 domain.

Molecular Dynamics: Each simulation system was solvated with an explicit TIP3P water model and neutralized by addition of Cl- or Na+ ions. The topology and coordinate files were prepared with the Amber *ff14SB*[33] force field. During MD simulations, two initial energy minimization runs were performed using a steepest descent algorithm of 50,000 steps. Subsequently, each system was gradually heated from 0 K to 300 K within 50 ps. This step was followed by another 50 ps equilibration run with a constant temperature of 300 K. After that, a 100 ns production run was carried out using the SHAKE algorithm[34] to constrain bonds involving hydrogen atoms. The minimization, heating, equilibration, and production runs were all applied using AMBER 16[35].

Binding Free Energy Calculations and Per-residue Free Energy Decomposition Analysis: From the 100 ns production run trajectory, 2000 frames were extracted between t=0-20 ns and t=80-100 ns, to calculate binding free energies. The Molecular Mechanics/Generalized Born Surface Area (MM/GBSA) method[36] was successfully employed using igb = 5 GB model in AMBER, which can be briefly summarized by the following equations:

$$\Delta G_{binding} = G_{complex} - G_{receptor} - G_{ligand} \quad (1)$$

$$\Delta G_{MM/GBSA} = E_{int} + E_{ele} + E_{vdW} + E_{polar} + E_{nonpolar} - T\Delta S \quad (2)$$

The binding free energy was calculated as the differences between free energy of the complex and the sum of the separate receptor and ligand shown in equation (1). The relative free energy DGMM/GBSA was estimated by the sum of every component in equation (2), with E_{int}, E_{ele} and E_{vdW} representing internal, electrostatic and van der Waals interactions; the solvation contribution is shown with E_{polar} and $E_{nonpolar}$. The TDS term represents the contribution of entropy which was not taken into account when calculating relative binding free energies in our study. To determine key residues involved in binding, a per-residue energy contribution was calculated and analyzed based on the same factors used in above calculations.

Statistical Analysis: All statistical analyses were computed using the GraphPad Prizm software. Kinetic data were analyzed by nonlinear regression using a three-parameter logistic function or an one-phase decay function. Statistical significance was accepted for p-value of <0.05. All data are presented as mean ± 1 standard deviation and are the result of at least two to three independent experiments, unless otherwise stated.

Results

Expression and Characterization of FV Variants. Previously we reported that ptFV retains full cofactor activity despite APC-catalyzed proteolysis[11,14]. APC cleaves the ptFV A2 domain at Lys507 and Arg742, homologous to human Arg506 and Arg709, respectively. Intriguingly, sequence analysis revealed the lack of a potential Arg306 cleavage site and a non-conserved sequence relative to mammalian FV consisting of ptFV residues 303-GNPDTLT-309 (**Figure 1A**). The GNPDTLT region is well-conserved in various snakes and reptile species, suggesting that the FV Arg306 cleavage site has been introduced at a later stage in evolution relative to Arg506. As the corresponding region is strictly conserved in mammals, we exchanged the ptFV residues GNPDTLT with the corresponding human Arg306 region (302-PKKTRNL-308) of constitutively active B-domainless hFV (**Figure 1B**) to generate the chimeric variants hFV-pt306 and ptFV-h306 (**Figure 1C**). Since a unique disulfide bond in ptFV covalently links the A2 and A3 domains[16], this structural element could potentially prevent A2 domain dissociation and ptFVa inactivation. To exclude the contribution of this disulfide bond to ptFVa inactivation, we generated an additional variant based on ptFV-h306 in which the cysteines involved were substituted by serines, generating ptFV-h306 S-S (**Figure 1C**). The FV variants were stably expressed in BHK cells and purified to homogeneity by ion-exchange chromatography. Each thrombin-activated FVa variant migrated on SDS-PAGE similar to recombinant wild-type hFVa or ptFVa (**Figure 1D**). In addition, SDS-PAGE analysis confirmed that the unique disulfide bond was preserved in ptFV-h306 but eliminated in ptFV-h306 S-S. Functional assessment of each FV variant

revealed a similar apparent affinity for their respective FXa species (**Table I** in the Data Supplement), indicating that substitution of the Arg306 region does not interfere with cofactor-FXa assembly.

ptFVa Variants Maintain Cofactor Function Upon Proteolysis by APC. We next assessed APC-mediated proteolysis of the ptFVa variants comprising the two major APC cleavage sites that are essential for the inactivation of mammalian FVa[21,24]. Thrombin-activated FVa variants were subjected to APC and the resulting cleavage pattern was analyzed by SDS-PAGE. While in hFVa variants full proteolysis was achieved in 15 min by 10 nM APC, high concentrations of APC (750 nM) were required for significant proteolysis of the ptFVa variants. As previously described[14], ptFVa was cleaved at Lys507 (**Figure IA** in the Data Supplement), which is equivalent to human Arg506. Conversely, we observed additional protein bands consistent with the cleavage of Arg306 in ptFVa-h306 (**Figure 2A**). N-terminal sequencing of the cleavage products confirmed the generation of a ptFVa variant comprising the homologous Arg306 and Arg506 cleavage sites (**Figure II** in the Data Supplement). Removal of the unique disulfide bond in ptFVa-h306 S-S did not affect the cleavage pattern relative to ptFVa-h306 (**Figure IB** in the Data Supplement). Moreover, while hFVa was proteolyzed at Arg306, Arg506, and Arg679 (**Figure IC** in the Data Supplement), an Arg306-like cleavage was absent in hFVa-pt306 (**Figure 2B**), demonstrating that the GNPDTLT region in ptFV is not targeted by APC.

Subsequently, the cofactor activity of the APC-proteolyzed FVa variants was assessed. Whereas hFVa was fully inactivated within 5 minutes, functional analysis employing a purified prothrombinase assay revealed partial inactivation of hFVa-pt306 by APC, in a manner similar to the previously characterized hFVa-Arg306Thr variant[37] (**Figure 2C**). Surprisingly, despite introduction of the Arg306 cleavage site and removal of the unique disulfide bond, both chimeric ptFVa variants maintained full cofactor activity during APC-treatment (**Figure 2C**). In addition, assessment of the ptFVa cofactor activity following an initial APC-treatment in the presence of protein S, a cofactor for APC[38,39], revealed identical results (**Figure 2D**). These findings indicate that the absence of a Arg306-like cleavage site and presence of ptFVa's unique disulfide bond do not contribute to the molecular mechanism that is at the basis of ptFVa's functional APC-resistance.

ptFV Retains Structural Integrity Following APC-mediated Proteolysis. APC-catalyzed proteolysis at the two major FVa cleavage sites Arg306 and Arg506 is known to result in A2 domain dissociation[24]. Since our ptFVa variants maintain full cofactor activity following APC-treatment, we hypothesized that despite selective proteolysis, A2 domain dissociation is prevented. Initial observations employing Native-PAGE analysis suggested

that APC-mediated proteolysis resulted in the fragmentation of hFV, whereas ptFV and ptFV-h306 S-S migrated as single molecules (**Figure SIII** in the Data Supplement). Intriguingly, our results show that non-proteolyzed hFV migrated as multiple species. Although the individual species could not be identified, this observation might be explained by the presence of impurities (~30 and 51 kDa, **Figure 2A**). Alternatively, these results could reflect partial glycosylation at Asn2181, leading to the 71/74 kDa hFVa light chain (Lane 1, **Figure 2A**)[40]. Nevertheless, the observation that APC-proteolyzed hFV migrates markedly different on native-PAGE relative to untreated hFV hints towards the fragmentation of the hFV protein. To explore the structural consequences of proteolysis in more detail we determined the structural integrity of the APC-treated ptFVa variants by size-exclusion chromatography. Following APC treatment, the proteolyzed FVa variants were applied to a 10 x 300 mm Superdex 200 Increase column and fractions were collected and analyzed by SDS-PAGE or Western blotting. In accordance with the native-PAGE, size-exclusion profiles suggested the fragmentation of APC-treated hFVa (**Figure 3A**), whereas a single elution peak was observed for APC-cleaved ptFVa (**Figure 3B**). The elution profile of APC-treated ptFVa-h306 S-S was comparable to that of ptFVa following APC treatment (**Figure 3C**), although an additional elution peak was observed as a result of impurities (**Figure 3F**). As expected from previous observations[24], the two hFVa A2 domain fragments Asn307-Arg506 and Gly507-Arg679 migrated separately from the rest of the molecule (A1-A3-C1-C2 domains) (**Figure 3D**). Conversely, ptFVa eluted as a single complex (**Figure 3E**), corroborating our functional data. Remarkably, despite introduction of the Arg306 region and deletion of the unique disulfide bond, ptFVa-h306 S-S retained structural integrity following proteolysis by APC (**Figure 3F**). The size-exclusion profile of ptFVa-h306 S-S displayed a shoulder in the elution peak which could indicate that the A2 domain has dissociated in a small portion of the total APC-treated FVa pool. As such, these results demonstrate that the dissociation of the ptFVa A2 domain is prevented by non-covalent interactions. Functional analysis of the chimeric FVa variants under conditions of high temperatures (**Figures IVA-B** in the Data Supplement) or high ionic strength (**Figure IVC** in the Data Supplement) did not reveal significant differences relative to wild-type FVa, suggestive of an enhanced A2 domain binding stability. Interestingly, proteolysis by the fibrinolytic serine protease plasmin revealed a striking decrease in ptFVa cofactor activity (**Figure VA** in the Data Supplement). While the loss of cofactor activity was comparable to wild-type FVa, all ptFVa variants retained up to 20% cofactor activity despite that full proteolysis was achieved within 5 minutes (**Figures VB-F** in the Data Supplement). These findings provide additional support for an enhanced structural stability of essential functional regions in ptFVa.

Stable Binding Free Energy for the A1-A2-A3 Domains of APC-proteolyzed ptFVa-h306 S-S during MD Simulations. In order to gain more insight into the structural stability of human and *P. textilis* FV, 100ns MD simulations were performed on hFVa and ptFVa-h306 S-S. The model of ptFVa-h306 S-S was generated from the X-ray structure of ptFV (PDB ID: 4BXS) in which 303-GNPDTLT-309 was substituted for the corresponding human Arg306 region and the Cys642-Cys1002 disulfide bond was disrupted. In addition, the peptide bonds that resemble Arg306 and Arg506/Lys507 cleavage were hydrolyzed in both FVa models to simulate an APC-proteolyzed state, and the C1-C2 domains were excluded from the MD simulations. Calculation of the free energies for the interaction between the A2 and A1-A3 domains revealed that these were comparable for hFVa and ptFVa-h306 S-S during the initial trajectory of the simulation (t=0-20ns), with a binding free energy of -76 ± 25 kcal/mole for hFVa and -76 ± 14 kcal/mole for ptFVa-h306 S-S (**Table 1**). However, in the final part of the MD trajectory (t=80-100ns), the binding free energy was remarkably increased to -39 ± 16 kcal/mole for hFVa, whereas a substantial decrease to -90 ± 14 kcal/mole was observed for ptFVa-h306 S-S. This suggests that over the course of the MD simulation, hFVa lost important interactions that facilitate the binding of the A2 to the A1-A3 domains. To examine these interdomain interactions in more detail, the binding free energies between the A2 and A1 or A2 and A3 domains were individually assessed. Interestingly, a loss of interaction between the A2 and A1 domains in hFVa was observed for the t=80-100ns interval (4 ± 10 kcal/mole, **Table 2**), while the binding free energy characterizing the A2-A3 interaction was nearly identical for both MD trajectories monitored. In contrast, the binding free energy between the A2-A1 or A2-A3 domains in ptFVa-h306 S-S remained unaffected during the simulations, indicative of a stable interaction. As such, these data confirm our *in vitro* studies by indicating that the structural integrity of the A1-A2-A3 domains in *P. textilis* FV is maintained following APC cleavage.

Stable Hydrogen Bond Pairs between the A2 and A1-A3 Domains Preserve A2 Domain Association in *P. textilis* FV. To further uncover the molecular mechanisms that are at the basis of the differential A2-A1 domain interactions observed for hFV and ptFV, the hydrogen bonds that contribute to the overall interdomain binding affinities were assessed. In accordance with the loss of A2-A1 domain interaction, the number of hydrogen bonds between the surfaces of the A2 and A1 domain in hFVa reduced over time during the MD simulations (**Figure 4A**). Representative structural snapshots revealed significant conformational changes in the A2 domain, suggesting that the A1 domain interacting regions are highly flexible following APC-catalyzed proteolysis (**Figures 4B-C**). In contrast, the number of hydrogen bonds formed between the A2 and A3 domains remained in a dynamic equilibrium during the simulation (**Figures 4D-F**), corroborating the stable A2-A3 binding affinity. The hydrogen bond formation

between the A2-A1 and A2-A3 domains in APC-proteolyzed ptFVa-h306 S-S appeared to be balanced and most hydrogen bonds persisted during the simulation (**Figures 4G-L**). These stable interactions might be explained by the conformational constraints of the A2 domain, since only minor structural changes in the binding surfaces were observed between structures at different timepoints. Identification of residues involved in key hydrogen bond interactions during >20% of the MD simulations demonstrated ptFVa-h306 S-S to accommodate a larger fraction of these interactions relative to hFVa (**Figure 5, Table SII** in the Data Supplement). Collectively, these findings indicate that ptFV comprises a high number of A2-A1 interactions that are preserved upon APC cleavage.

A Unique Loop Conformation in the A2 Domain Prevents A2 Domain Dissociation in *P. textilis* FV. Structural comparison of the MD simulations revealed that the A2 domain of hFVa and ptFVa-h306 S-S adopt strikingly different conformations (**Figure 4**). In hFVa, we observed a major conformational change in a surface-exposed A2 domain loop (loop2) that is extended into the solvent and interacts with an A1 domain loop (loop1) via one stable interaction pair (Glu20-Arg439; **Figures 4, VA** in the Data Supplement). While human and *P. textilis* FVa share 55% sequence identity, the positioning of loop1 and loop2 is conserved (**Figure SVI** in the Data Supplement). In addition, sequence analysis showed that loop2 is well-conserved in reptiles, whereas a significantly different sequence is conserved in mammalian FV (**Figure SVII** in the Data Supplement). Interestingly, MD simulations in ptFVa-h306 S-S indicated that loop2 is more compact and does not interact with loop1 (**Figures 4,5B**). Supporting the structural observations, assessment of the solvent accessible surface area (SASA) of individual A domains or A domain complexes over the MD trajectories further revealed that the SASAs of ptFVa-h306 S-S were smaller relative to hFVa (**Figure SVIII** in the Data Supplement). This was found to be the result of a more compact A2 domain, as compared to the A1-A3 domains. To specifically determine the role of loop2 in A2 domain stability, we created an *in silico* chimeric hFVa structure in which the human loop2 was exchanged for the homologous ptFV loop2 region (hFVa-ptloop2), upon which a 100ns MD simulation was performed (**Figure 6A**). As substitution of loop2 destabilized the structure and required several nanoseconds to adopt a stable state, we excluded the initial 20ns from our analysis. Intriguingly, the A2 domain binding free energy in hFVa-ptloop2 was markedly decreased relative to hFVa (hFVa-ptloop2, -64 kcal/mole; hFVa, -39 kcal/mole), although it remained higher compared to ptFVa-h306 S-S (**Table 1**). In similar fashion, exchange of loop2 substantially decreased the average A2 domain SASA (15846.2 ± 0.05 $Å^2$) as compared to hFVa (16689.3 ± 0.04 $Å^2$), but remained larger relative to ptFVa-h306 S-S (14761.8 ± 0.04 $Å^2$), illustrating the compact conformation of the ptFV loop2. Consistent with these findings, the A2-A1 domain hydrogen bonds were stabilized in chimeric

hFVa-ptloop2, while the exchange of loop2 did not affect the interactions between the A2 and A3 domains (**Figures 6B-D**). Nonetheless, we cannot exclude that differences in hydrogen bond pairing between the A2 and A3 domains contribute to the decreased binding free energy for A2 domain binding in hFVa-ptloop2. Collectively, this structural bioinformatics analysis indicates that the compact and inflexible ptFV loop2 stabilizes the surface interactions between the A2 and A1 domains following APC proteolysis and could provide a mechanism that prevents A2 domain dissociation in ptFVa.

Discussion

One of the essential characteristics underlying any hemostatic response is the timely inactivation of proteases and cofactors following proteolytic activation of their respective substrate. The specialized mechanisms of the anticoagulant system thereby prevent uncontrolled blood clotting and life-threatening thrombotic events. Our work, amongst others[11,14,18], highlights the importance of strict regulatory pathways for FV and shows that bypassing these mechanisms can be used as a potent weapon to gain evolutionary advantages.

We previously speculated that absence of the Arg306 cleavage site, required for the inactivation of mammalian FVa, is at the basis of the functional APC-resistance in ptFVa[14,18]. To test this hypothesis, chimeric ptFV variants were generated that lack the unique A2-A3 domain disulfide bond and/or comprise the human Arg306 region. Our functional assessments show that despite Arg306 cleavage and disruption of the unique disulfide bond, ptFVa retains cofactor activity upon APC-catalyzed proteolysis. As such, our findings demonstrate that these elements in ptFV do not play a role in the functional resistance to APC.

Liver-derived ptFV shares 96% sequence identity to its venom paralog[41] and we previously revealed that liver-expressed ptFV shares the procoagulant characteristics of venom-derived ptFV, including the functional resistance to APC[18]. These observations raise fundamental questions on the hemostatic regulatory mechanisms in *P. textilis*. It is currently unknown whether Elapidae express protein C, but if so, it would be of interest to characterize the mechanistic principles that hallmark the anticoagulant response in these snakes. It is also important to note that Arg306 is only conserved in mammals, whereas lower vertebrates do not seem to comprise an homologous Arg306 cleavage site. This indicates that lower vertebrates have a distinct mechanism to inactivate FVa. It has been suggested that reptiles have a primitive intrinsic coagulation pathway and a complete lack of factor XI and factor XII[42-46]. The absence of these factors may favor a more procoagulant system that is required to generate sufficient amounts of

thrombin. Interestingly, our findings revealed that similar to human FVa[47,48], plasmin was able to proteolyze and significantly reduce the cofactor activity of ptFVa, although a 20-fold higher plasmin concentration was required to obtain fully proteolyzed ptFVa. Considering that the plasma concentration of plasminogen is ~2 μM[49], these results could suggest that plasmin plays a physiological role in the regulation of liver-expressed ptFVa. Since the generation of plasmin is taking place at a later stage of hemostasis relative to the activation of protein C, these results may support the hypothesis that liver-expressed ptFV has a more procoagulant role. In contrast, liver- and venom-derived ptFX share ~76% sequence identity[50]. This may indicate that venom-derived ptFX underwent evolutionary adaptations in order to circumvent negative regulatory mechanisms and could potentially suggest that the activity of the liver-expressed ptFVa-ptFXa complex is primarily regulated by antithrombin or tissue factor pathway inhibitor.

Using size-exclusion chromatography, we showed that despite APC-mediated proteolysis A2 domain dissociation in ptFVa is prevented. Remarkably, the A2 domain remained associated following introduction of the Arg306 cleavage site in ptFVa. Attempts to weaken the non-covalent structural integrity of the APC-treated ptFVa variants failed to significantly impact their ability to function as cofactor for ptFXa. These results demonstrate that following selective proteolysis ptFVa maintains structural integrity mediated by strong non-covalent interactions. Strikingly, these findings contradict our current understanding of FVa inactivation[51] and imply the presence of unique structural elements that prevent A2 domain dissociation in ptFVa.

In an attempt to unravel the mechanistic principles of A2 domain association, we identified a potential crucial role for A1-A2 domain interactions. In hFVa, the binding free energy between the A1 and A2 domain increases drastically upon APC-mediated proteolysis. As a consequence, the interaction between the A1 and A2 domain is lost which seemingly triggers the dissociation of the A2 domain. The loss of A1-A2 domain binding affinity coincides with a major conformational change in the hFVa loop2. This highly flexible loop engages in weak interactions with the A1 domain loop1 and facilitates several A1-A2 domain hydrogen bonds. Upon APC-catalyzed proteolysis, the number of hydrogen bonds between the surfaces of the A2 and A1 domains reduces as a result of the conformational changes in the A2 domain. Conversely, the A1-A2 domain binding free energy remains stable following APC-catalyzed cleavage of ptFVa. In contrast to hFVa, the ptFVa loop2 does not interact with loop1 and adopts a rigid conformation that is stabilized by several key hydrogen bonds. Exchange of the ptFV loop2 to hFVa significantly improved the binding affinity between the A2 and A1-A3 domains, providing further support for the central role of loop2 in the A2 domain association. Interestingly, loop2 is located directly distal from the Arg306 cleavage site,

which may suggest that the stable non-covalent interactions are able to compensate for Arg306 cleavage. Additionally, it is possible that ptFXa comprises a structural element that supports the functional APC resistance of ptFVa. Productive interactions between the proteolyzed ptFVa A2 domain and ptFXa could stabilize the conformation of ptFVa in such way that it is able to fulfill its role as cofactor. Moreover, the anionic membrane layer could be another stabilizing factor that allows for cofactor activity following APC-proteolysis. Although the ptFVa-ptFXa complex is able to convert prothrombin in the absence of membranes, it is currently unknown whether functional resistance to APC is maintained when anionic phospholipids are absent. Previous reports proposed that binding of FVa to anionic phospholipids induces conformational changes in the A2 domain that present a FXa interaction site[52,53]. Whether such interactions are required for the procoagulant enhancements in ptFVa remains to be determined.

Overall, characterization of the mechanistic principles and identification of key regions or residues responsible for ptFV's functional resistance to APC could provide unique opportunities for the generation of novel stable FV variants. Our findings might suggest that substitution of human loop2 for the corresponding region in ptFV could create a human FV variant with an improved intrinsic stability resulting from the increased A1-A2 domain binding affinity. Such a FV variant could have an additional advantage over previously reported Arg306Gln/Arg506Gln FV variants, since it will retain procoagulant activity independent of potential APC cleavage. It has been reported that mutation of the three APC cleavage sites in FVa results in FVa inactivation via APC-mediated proteolysis at alternative positions in the A2 domain[29,54]. Moreover, FV has an important role as cofactor for APC in the inactivation of factor VIIIa[55], a crucial reaction to downregulate the procoagulant response[56]. This anticoagulant role is dependent on the cleavage of Arg506 by APC[57,58] and as such this function is absent in Arg506-mutated FV variants.

In conclusion, our findings highlight the exceptional structural features that have converted ptFV into an extremely procoagulant protein. Here we demonstrated that ptFVa maintains functional resistance to APC despite introduction of the Arg306 cleavage site, in sharp contrast to the APC response of mammalian FVa. To do so, ptFV has uniquely adapted non-covalent interactive regions in the A1 and A2 domains that stabilize the A2 domain following proteolysis by APC. Taken together, our findings provide evidence for a unique structural element by which ptFV circumvents the regulatory mechanisms and shed new insights on the mechanistic principles of A2 domain dissociation and FVa inactivation.

Figures

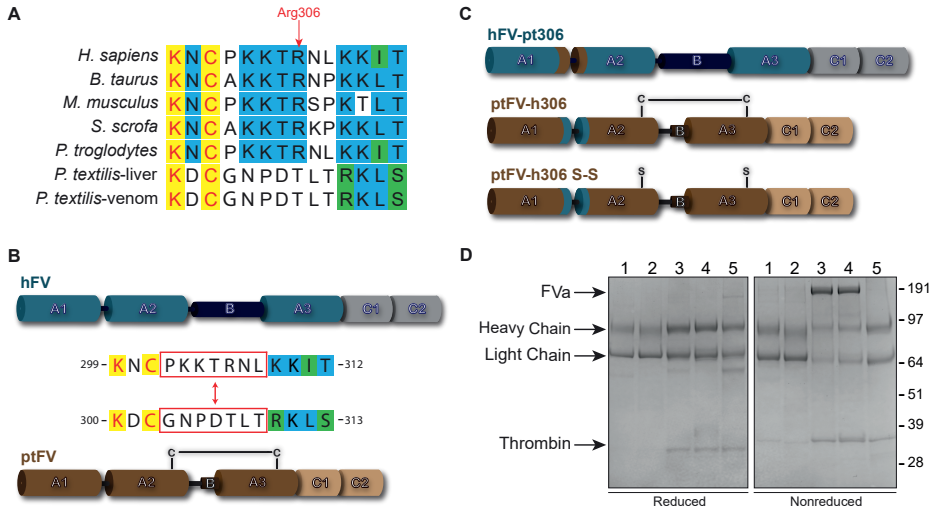

Figure 1. Generation and SDS-PAGE analysis of purified factor Va variants. (A) Sequence alignment of the Arg306 region. Completely conserved residues are highlighted in yellow, partly conserved residues in blue, and residues belonging to the same classification are indicated in green. **(B)** Schematic representation of B domain truncated human FV (hFV) and venom-derived *P. textilis* FV (ptFV). The Arg306 region indicated by the red boxes was exchanged between hFV and ptFV. **(C)** Schematic representation of generated FV variants. Human regions are indicated in blue/grey, ptFV regions are brown/beige. Swapping the Arg306 region generated hFV-pt306 and ptFV-h306. Additional removal of the disulfide bond by replacing the cysteines (Cys642 and Cys1002) for serines in ptFV generated ptFV-h306 S-S. **(D)** SDS-PAGE of purified thrombin-activated FVa variants (2 µg per lane) under reducing (left panel) and non-reducing (right panel) conditions visualized by staining with Coomassie Brilliant Blue R-250. Lane 1, hFVa; lane 2, hFVa-pt306; lane 3, ptFVa; lane 4, ptFVa-h306; lane 5, ptFVa-h306 S-S. Relevant fragments and the apparent molecular weights of the standards are indicated.

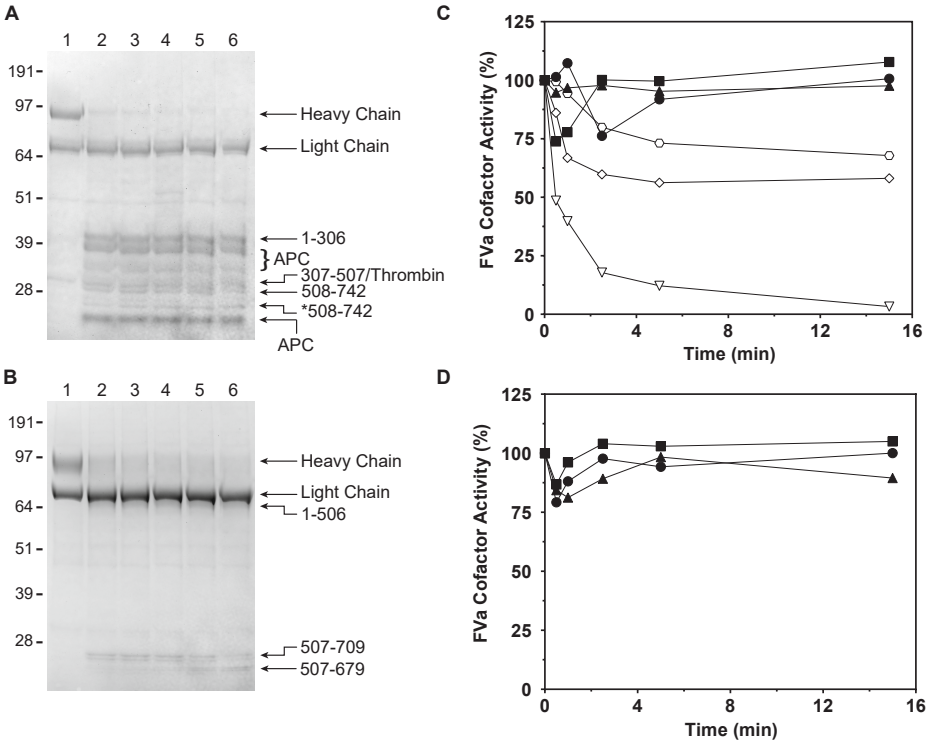

Figure 2. Activated protein C-mediated proteolysis of human and *P. textilis* factor Va variants. (A-B) SDS-PAGE of activated protein C (APC)-treated ptFVa-h306 **(A)** and hFVa-pt306 **(B)** (3 µg per lane) under reducing conditions and visualized by staining with Coomassie Brilliant Blue R-250. Lanes 1-6 represent time samples quenched at 0, 0.5, 1, 2.5, 5, and 15 min. Relevant FVa fragments and the apparent molecular weights of the standards are indicated. We hypothesize that *508-742 is cleaved at a C-terminal position because its N-terminal sequence was determined to be the same as 508-742 (see Supplementary Figure II). **(C-D)** Reaction mixtures containing **(C)** 50 µM PCPS and 500 nM hFVa (open triangles), hFVa-pt306 (open diamonds), or hFVa-Arg306Thr (open hexagons) were incubated with 10 nM APC and similar mixtures containing 500 nM ptFVa (closed circles), ptFVa-h306 (closed squares) or ptFVa-h306 S-S (closed triangles) were incubated with 750 nM APC. In addition, similar reactions containing **(D)** PCPS (50 µM) and ptFVa variants (50 nM) were treated with 75 nM APC in the presence of protein S (100nM). **(C-D)** At selected time intervals, samples were removed for cofactor activity by determining the initial velocity of prothrombin conversion. The data are representative of three independent experiments.

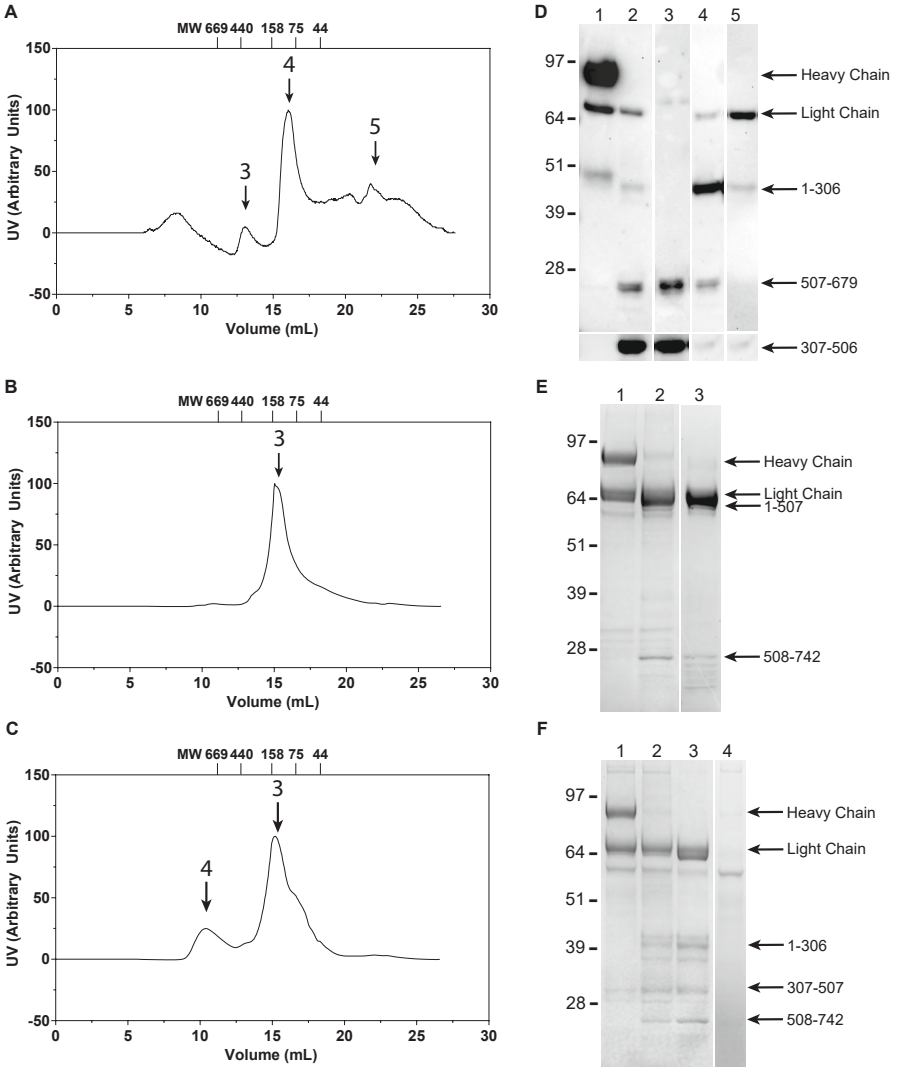

Figure 3. Size-exclusion chromatography of activated protein C-treated FVa variants. (A-C) Size-exclusion elution profiles of APC-treated hFVa **(A)**, ptFVa **(B)**, or ptFVa-h306 S-S **(C)** performed as detailed in 'Materials and Methods'. Arrows and numbers indicate the respective fractions shown in **D-F**. MW, molecular weight. **(D)** Western blot analysis of hFVa under reducing conditions following proteolysis by APC and size-exclusion chromatography elution. Lane 1, thrombin-activated hFVa; lane 2, APC-treated hFVa; lane 3, A2 domain fraction; lane 4, A1-A3-C1-C2 and A2 domain fraction; lane 5, A1-A3-C1-C2 domains fraction. **(E-F)** SDS-PAGE of APC-treated ptFVa **(E)** or ptFVa-h306 S-S **(F)** following size-exclusion chromatography under reducing conditions and visualized by staining with Coomassie Brilliant Blue R-250. Lanes 1, thrombin-activated ptFVa variant; lanes 2, APC-treated ptFVa variant; lanes 3 and 4, elution fractions indicated by the black arrows and numbers in **B-C**. Relevant FVa fragments and the apparent molecular weights of the standards are indicated. The data are representative of two independent experiments. Panels **D-F** are composed of two Western Blots or SDS-PAGE gels, respectively.

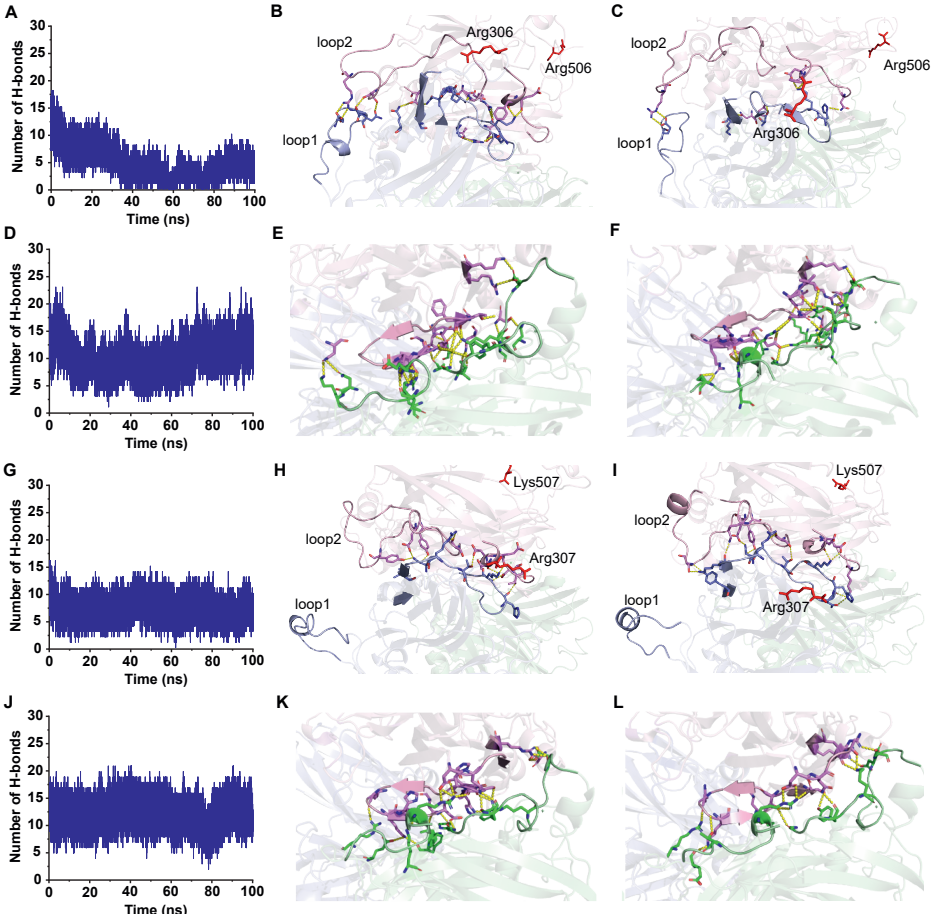

Figure 4. Comparison of interdomain hydrogen bonds between surfaces of the A2 and the A1/A3 domains in human and *P. textilis* FV. The structural conformation and interdomain hydrogen bonds between the surfaces of the A2 and A1 **(B-C, H-I)** or A2 and A3 **(E-F, K-L)** domains are shown at the start (t=0ns) **(B, E, H, K)** and end (t=100ns) **(C, F, I, L)** of the hFVa **(B-C, E-F)** and ptFVa-h306 S-S **(H-I, K-L)** MD simulations. The A1, A2, and A3 domains are indicated in blue, pink, and green, respectively. Residues that engage in hydrogen bond formation and the APC cleavage sites (hFVa, Arg306, Arg506; ptFVa, Arg307, Lys507) are shown in stick configuration, with the latter highlighted in red. Hydrogen bonds are indicated by the yellow dashed lines. The A1 domain loop1 and A2 domain loop2 represent the identified unique loop conformations. **(A, D, G, J)** Interdomain hydrogen bonds between the A2 and A1 **(A, G)** or A2 and A3 **(D, J)** domains were quantified during a 100ns MD simulation of hFVa **(A, D)** and ptFVa-h306 S-S **(G, J)**.

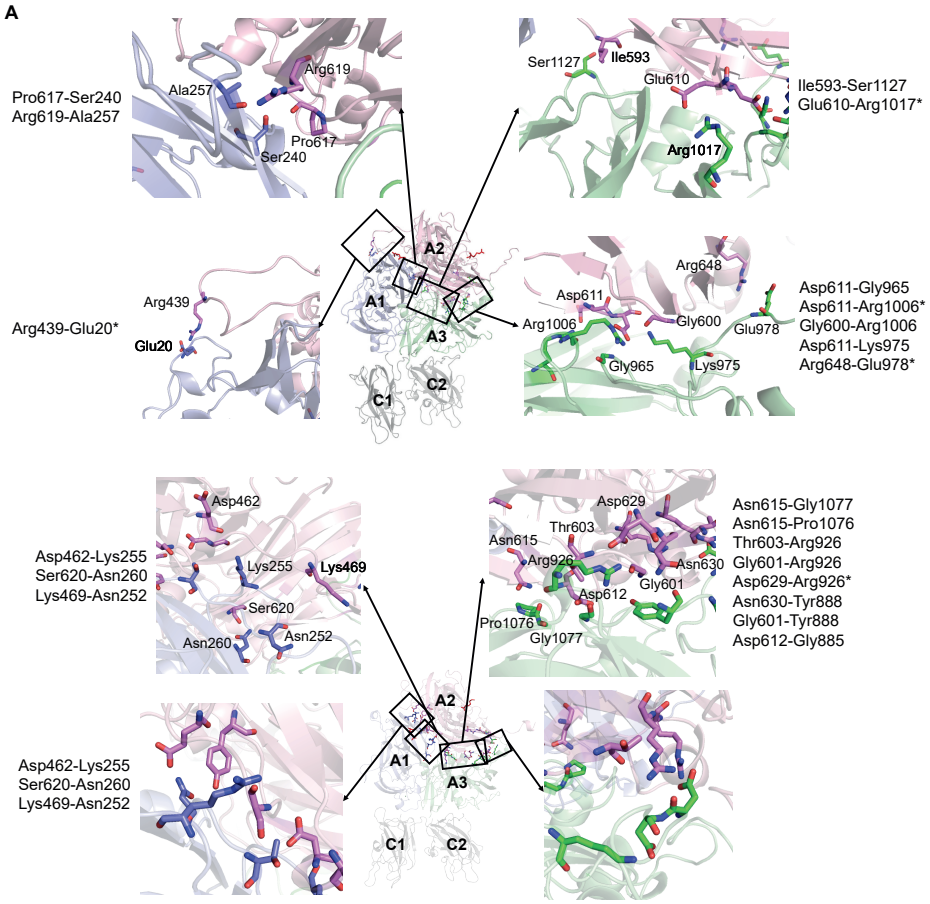

Figure 5. Structural representation of residues involved in key A2-A1 or A2-A3 domain hydrogen bond interaction pairs. (A-B) Residues involved in key hydrogen bond interactions, as defined in 'Materials and Methods', between the A2 domain (pink) and the A1 (blue) or A3 domain (green) in hFVa **(A)** or ptFV **(B)**, and the APC cleavages sites (Arg306, Arg506) are shown in stick configuration, with the latter highlighted in red. The inserts display zoomed-in regions and depict the interaction pairs. The A1, A2, A3, C1, and C2 domains are indicated. * Denotes charged interactions.

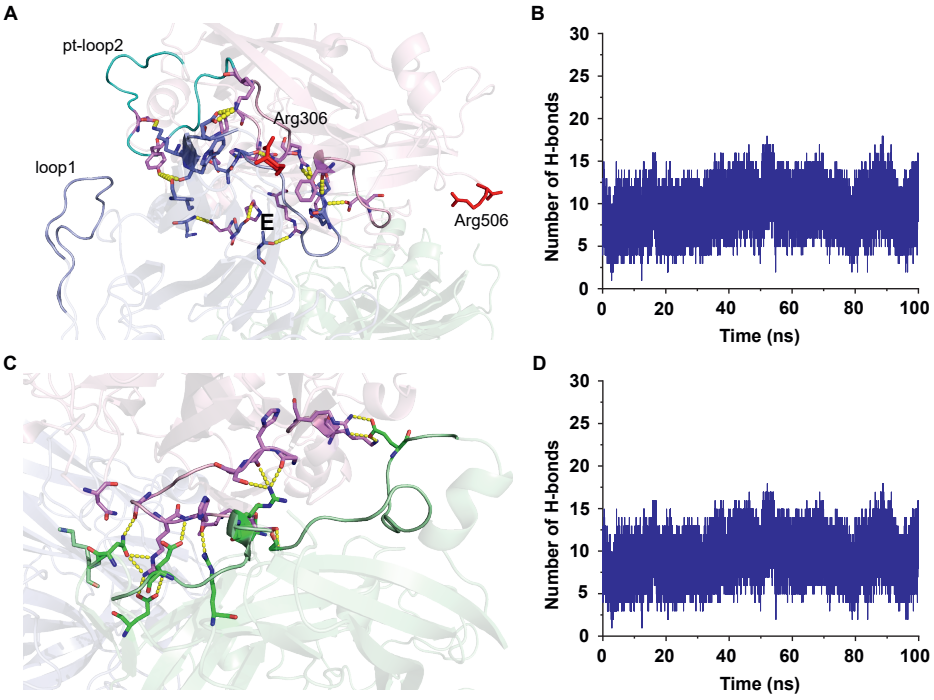

Figure 6. Stable hydrogen bond formation between the A2 and A1 domains upon substitution of human loop2 for the corresponding region in *P. textilis* FV. *In silico* exchange of loop2 in hFVa for the homologous loop2 in ptFV generated a chimeric hFVa variant. **(A, C)** Interdomain hydrogen bonds between the surfaces of the A2 and A1 **(A)** or A2 and A3 **(C)** domains are shown in a representative snapshot of the 100ns MD simulation of chimeric hFVa. The A1, A2, and A3 domains are indicated in blue, pink, and green, respectively. Residues that engage in hydrogen bond formation and the APC cleavage sites (Arg306, Arg506) are shown in stick configuration, with the latter highlighted in red. Hydrogen bonds are indicated by the yellow dashed lines. **(B, D)** Interdomain hydrogen bonds between the A2 and A1 **(B)** or A2 and A3 **(D)** domains were quantified during a 100ns MD simulation of the chimeric hFVa model.

MD trajectory	hFVa (kcal/mole)	ptFVa-h306 S-S (kcal/mole)	hFVa-ptloop2 (kcal/mole)
0-20ns	-75.46 ± 24.99	-75.58 ± 13.68	N.A.
80-100ns	-39.36 ± 15.57	-90.47 ± 13.51	-63.53 ± 15.89

Table 1. The binding free energies of the A2 and A1-A3 domain interaction. Binding free energies were calculated using the MD trajectory from t=0-20ns or t=80-100ns as described in 'Materials and Methods'. N.A., For hFVa-ptloop2 the t=0-20ns trajectory was excluded from the analysis due to the initial destabilization of the structure following loop exchange. Energies are expressed as kcal/mole ± S.D.

MD trajectory	Domain	hFVa (kcal/mole)	ptFVa-h306 S-S (kcal/mole)
0-20ns	A2-A1	-37.20 ± 15.69	-41.37 ± 9.71
	A2-A3	-43.45 ± 13.41	-41.55 ± 9.20
80-100ns	A2-A1	4.37 ± 10.39	-36.44 ± 8.98
	A2-A3	-46.69 ± 10.40	-55.39 ± 10.12

Table 2. Binding free energies for the binding of the A2 domain to the A1 or A3 domain. Binding free energies were calculated using the MD trajectory from t=0-20ns or t=80-100ns as described in 'Materials and Methods'. Energies are expressed as kcal/mole ± S.D.

Supplemental Methods

Plasmin-mediated Inactivation of FVa Variants: Plasmin-mediated proteolysis was achieved using FVa variants (500 nM) in the presence of PCPS (50 μM) and addition of plasmin (hFVa 20 nM; ptFVa 400 nM) at 37 °C. Aliquots of the reaction mixtures were withdrawn at the indicated time intervals and analyzed by SDS-PAGE and through assessment of the residual FVa cofactor activity. Activity assay mixtures contained prothrombin (1.4 μM), PCPS (50 μM), DAPA (10 μM), plasmin-proteolyzed hFVa (0.2 nM) or ptFVa variants (0.1 nM), and FXa (2 nM) or ptFXa (1 nM), respectively. Prothrombin activation was determined as described[27].

Thermal Decay of APC-treated FVa Variants: Thrombin-activated ptFV variants (100 nM) were treated with APC (150 nM) in the presence of PCPS (50 μM) for 15 minutes at 37°C and were subsequently incubated in a water bath at 52°C. At indicated timepoints, an aliquot was withdrawn and diluted in assay buffer on ice. Cofactor activity of FVa aliquots were measured using assay mixtures containing prothrombin (1.4 μM), PCPS (50 μM), DAPA (10 μM), APC-proteolyzed ptFVa (0.2 nM) and ptFXa (1 nM). Prothrombin activation was determined as described[27].

Stability of APC-treated FVa Variants at Increased Ionic Strength: Thrombin-activated ptFVa-h306 S-S (50 nM) was treated with APC (75 nM) for 5 hours at 37°C in the presence of PCPS (50 μM) and increasing concentrations of NaCl (150-2000 mM) in assay buffer Cofactor activity of FVa aliquots were measured using assay mixtures containing prothrombin (1.4 μM), PCPS (50 μM), DAPA (10 μM), APC-proteolyzed ptFVa-h306 S-S (0.1 nM) and ptFXa (1 nM). Prothrombin activation was determined as described[27].

Native PAGE: The structural integrity of FV variants was assessed by Native-PAGE using pre-cast 3-12% Bis-Tris gels (Life technologies; Carlsbad, CA, USA). APC-proteolyzed FV variants were loaded on gels using Native Sample Buffer (Life technologies; Carlsbad, CA, USA) followed by staining with Coomassie Brilliant Blue R-250.

Supplemental Figures

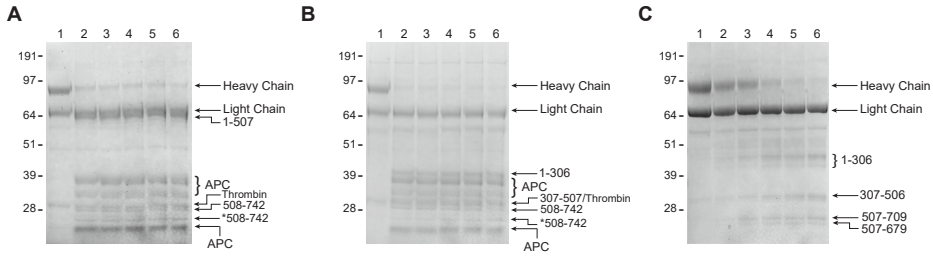

Supplementary figure I. Activated protein C (APC) treatment of human and *P. textilis* factor Va variants. SDS-PAGE of APC-treated ptFVa **(A)**, ptFVa-h306 S-S **(B),** or hFVa **(C)** (3 µg per lane) under reducing conditions and visualized by staining with Coomassie Brilliant Blue R-250. Lanes 1-6 represent time samples quenched at 0, 0.5, 1, 2.5, 5, and 15 min. Relevant fragments including the heavy chain (A1-A2) and light chain (A3-C1-C2) and the apparent molecular weights of the standards are indicated. We hypothesize that *508-742 is cleaved at a C-terminal position because its N-terminal sequence was determined to be the same as 508-742 (see Supplementary Figure 2). The data are representative of two to three independent experiments.

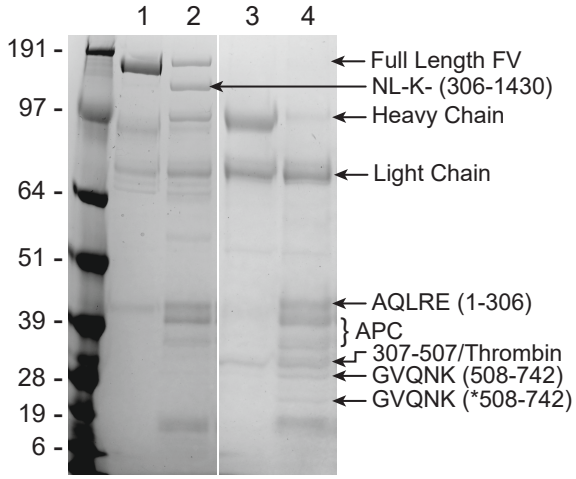

Supplementary figure II. Characterization of APC cleavage sites in ptFV-h306. SDS-PAGE of APC-treated ptFV-h306 and ptFVa-h306 (3 µg per lane) under reducing conditions and visualized by staining with Coomassie Brilliant Blue R-250. Lane 1, ptFV-h306 at t=0; lane 2, ptFV-h306 at t=0.5min; lane 3, ptFVa-h306 at t=0; lane 4, ptFVa-h306 at t=0.5min. N-terminal sequence results of the indicated protein bands and the apparent molecular weights of the standards are shown.

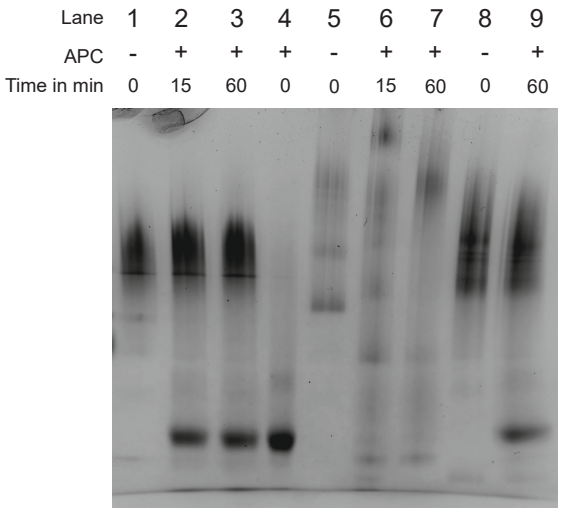

Supplementary figure III. Native-PAGE analysis of APC-proteolyzed human and *P. textilis* factor V variants. Lane 1, ptFV at t=0 min; lane 2, APC-treated ptFV at t=15 min; lane 3, APC-treated ptFV at t=60 min; lane 4, APC; lane 5, hFV at t=0 min; lane 6, APC-treated hFV at t=15 min; lane 7, APC-treated hFV at t=60 min; lane 8, ptFV-h306 S-S at t=0 min; lane 9, APC-treated ptFV-h306 S-S at t=60 min. The data are representative of two independent experiments.

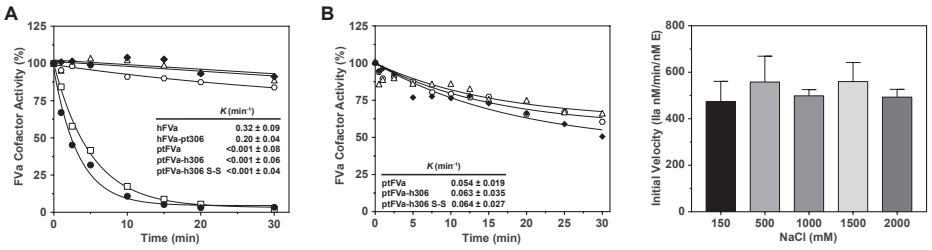

Supplementary figure IV. Factor Va cofactor activity in conditions of increased temperature or high ionic strength. (A) Reaction mixtures containing 20 nM hFVa (closed circles), hFVa-pt306 (open squares), ptFVa (closed diamonds), ptFVa-h306 (open triangles), or ptFVa-h306 S-S (open hexagons) were incubated at 52°C. At selected time intervals, samples were removed and diluted on ice, upon which they were assayed for cofactor activity employing a FV-specific PT-based clotting assay. **(B)** APC-treated ptFVa (closed diamonds), ptFVa-h306 (open triangles), or ptFVa-h306-SS (open hexagons) were incubated at 52°C. At selected time intervals, samples were removed and diluted on ice, upon which they were assayed for cofactor activity by determining the initial velocity of prothrombin conversion as described in 'Materials and Methods'. Cofactor decay rate constants ± 1 S.D. (insets) were determined by fitting the data to a one-phase decay function by non-linear regression. The data are representative of two to three independent experiments. **(C)** ptFVa-h306 S-S (50 nM) was treated with APC (75 nM) at 37°C in the presence of 50 μM PCPS and increasing concentrations of NaCl (150-2000 mM) in assay buffer. After 5 hours of incubation, samples were removed and diluted in assay buffer for cofactor activity assessment by determining the initial velocity of prothrombin conversion. Data represent the mean ± 1 S.D. and are representative of two independent experiments.

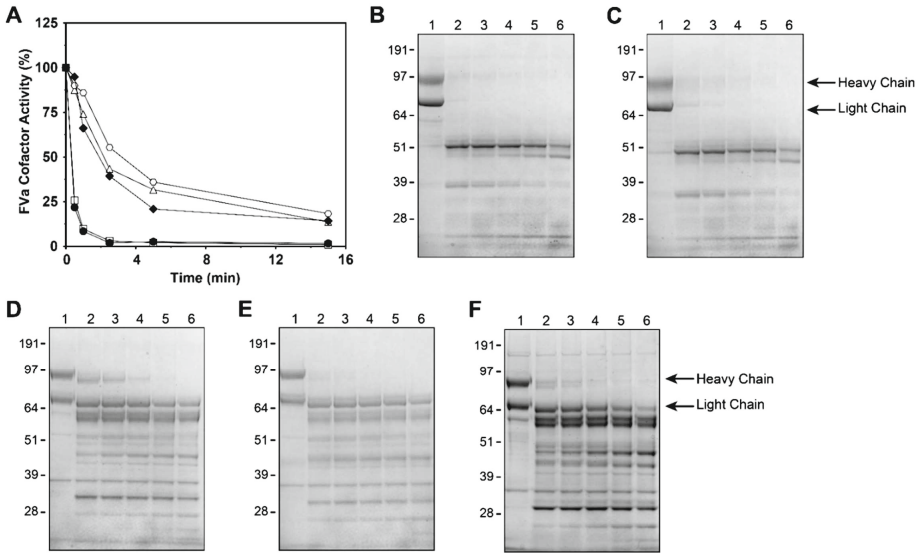

Supplementary figure V. Plasmin treatment of human and *P. textilis* factor Va variants. (A) Reaction mixtures containing 50 µM PCPS and 500 nM hFVa (closed circles) or hFVa-pt306 (open squares) were incubated with 20 nM plasmin, and similar mixtures containing ptFVa (closed diamonds), ptFVa-h306 (open hexagon), or ptFVa-h306 S-S (open triangles) were incubated with 400 nM plasmin. At selected time intervals, samples were taken and assessed for cofactor activity by determining the initial velocity of prothrombin conversion as detailed in 'Materials and Methods'. The data are representative of two to three independent experiments. SDS-PAGE analysis of plasmin-treated hFVa **(B)**, hFVa-pt306 **(C)**, ptFVa **(D)**, ptFVa-h306 **(E)**, or ptFVa-h306 S-S **(F)** (3 µg per lane) under reducing conditions and visualized by staining with Coomassie Brilliant Blue R-250. Lanes 1-6 represent samples quenched at 0, 0.5, 1, 2.5, 5, and 15 min. The FVa heavy (A1-A2 domains) and light (A3-C1-C2 domains) chains and the apparent molecular weights of the standards are indicated. The data are representative of two to three independent experiments.

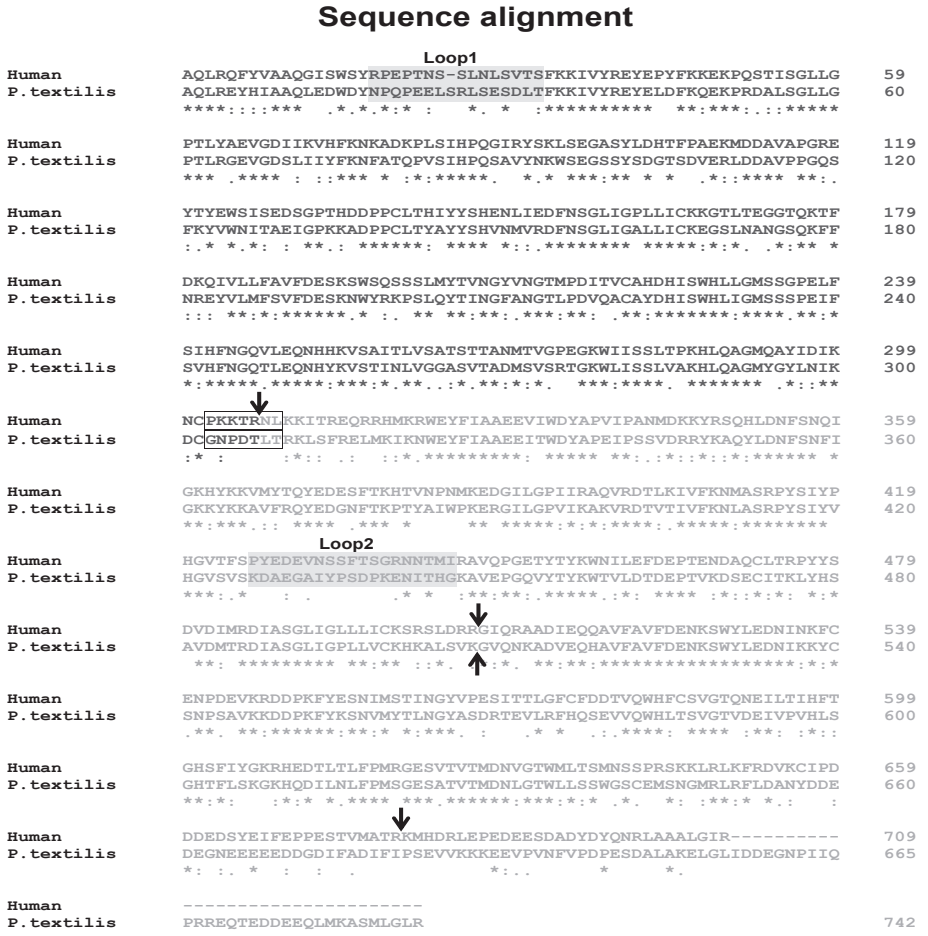

Supplementary figure VI. Sequence alignment of the human and *P. textilis* A1-A2 domains in FVa. "*" represents identical amino acids, ":" represents very similar amino acids, "." represents somewhat similar amino acids. The A1, A2, and A3 domains are indicated in blue, pink, and green, respectively. The Arg306 region is indicated by the black frame and loop1 and loop2 are highlighted in yellow. Black arrows indicate APC cleavage sites.

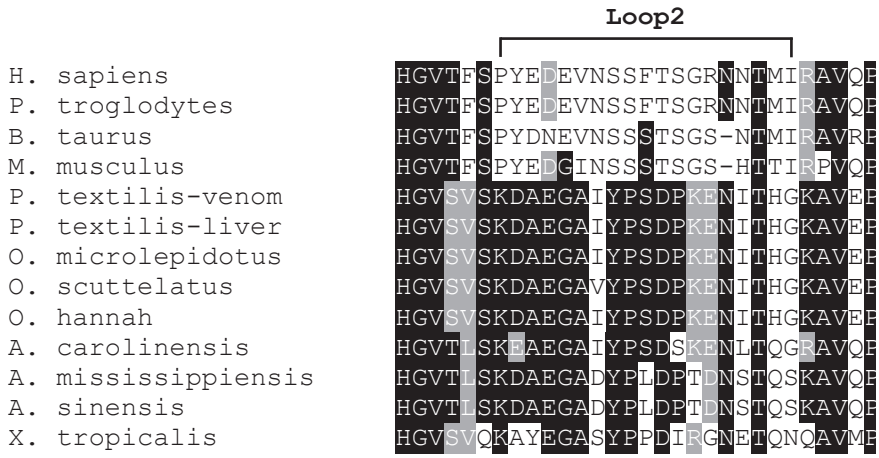

Supplementary figure VII. Sequence alignment of the A2 domain loop2 in FV. Alignment of the amino acid sequences comprising the FV A2 domain loop2 (Clustal Omega Module; EMBL-EBI, UK). Residues identical to the consensus are shown in black; residues similar to the column consensus are shown in grey. The amino acids corresponding to the A2 domain loop2 are indicated.

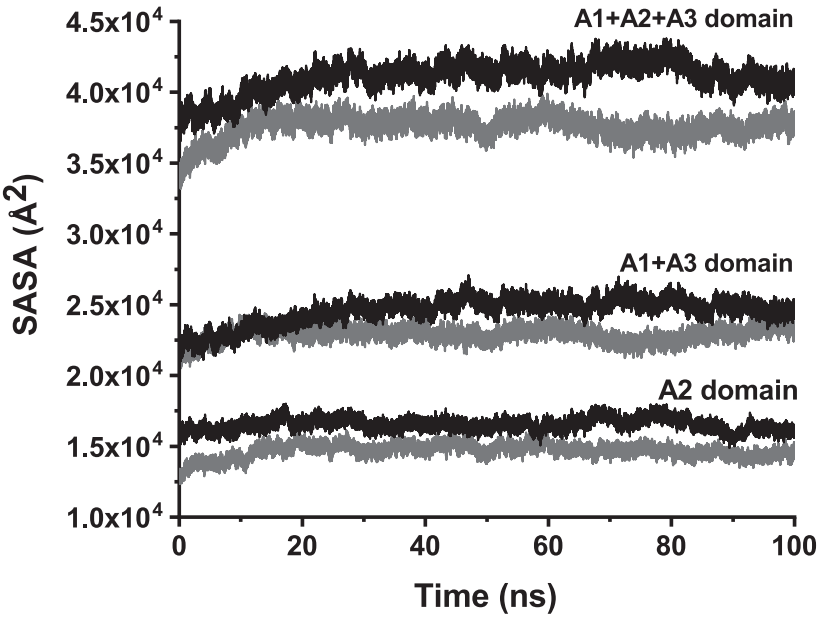

Supplementary figure VIII. Solvent accessible surface areas (SASA) in human and *P. textilis* FV. The SASA of the A2 domain, the A1 and A3 domain complex, and the A1, A2, and A3 domain complex were calculated as described in 'Materials and Methods'. The black and red lines represent human and *P. textilis* FV, respectively.

	hFV	hFV-pt306	ptFV	ptFV-h306	ptFV-h306 S-S
$K_{d,\ app}$ (nM)	0.71 ± 0.20	0.97 ± 0.20	0.83 ± 0.18	0.48 ± 0.16	0.97 ± 0.29

Supplementary table I. Apparent binding affinity for the cofactor. The apparent binding affinity of hFXa or ptFXa for their respective cofactor species was obtained as described in 'Materials and Methods'. The mean values ± S.D. are representative of two to three independent experiments.

Binding surfaces	hFVa	ptFVa-h306 S-S	hFVa-ptloop2
A2-A1	Arg439-Glu20* Pro617-Ser240 Arg619-Ala257	Lys469-Asn252 Glu430-Asn245 Tyr419-Asn245 Asp464-Thr248 Asp462-Lys255 Ser620-Asn260 Ser424-Arg275	Arg475-Lys254 Gly421-Gly245 Tyr418-Asn244 Asp469-Lys254* Asp480-Asn244 Tyr433-Trp278 Phe462-Lys254 Asp480-Ser281 Pro617-Ser240 Asn591-Lys286 Glu621-His253 Arg619-Thr259
A2-A3	Ile593-Ser1127 Asp611-Gly965 Arg648-Glu978* Asp611-Arg1006* Glu610-Arg1017* Gly600-Arg1006 Asp611-Lys975*	Gly601-Arg926 Asn630-Tyr888 Asp629-Arg926* Asp612-Gly885 Thr603-Arg926 Asn615-Gly1077 Asn615-Pro1076 Arg649-Asp898* Arg651-Asp898* Gly601-Tyr888 Thr633-Lys890 Arg651-Asp899*	Ile593-Ser1127 Asp611-Arg1006* Asp611-Gly965 Glu610-Arg1017* Asn467-Asn1145 Arg608-Glu1143* His609-Glu1010 Arg648-Glu978*

* Denotes the charged interactions

Supplementary table II. Key hydrogen bond interaction pairs between the A2 domain and the A1 or A3 domain. Hydrogen bond pairs were identified as described in 'Materials and Methods'.

References

1 Owren, P. A. Parahaemophilia; haemorrhagic diathesis due to absence of a previously unknown clotting factor. *Lancet* **1**, 446-448 (1947).
2 Camire, R. M. & Bos, M. H. The molecular basis of factor V and VIII procofactor activation. *J Thromb Haemost* **7**, 1951-1961, doi:10.1111/j.1538-7836.2009.03622.x (2009).
3 Bos, M. H. & Camire, R. M. A bipartite autoinhibitory region within the B-domain suppresses function in factor V. *J Biol Chem* **287**, 26342-26351, doi:10.1074/jbc.M112.377168 (2012).
4 Schreuder, M., Reitsma, P. H. & Bos, M. H. A. Blood coagulation factor Va's key interactive residues and regions for prothrombinase assembly and prothrombin binding. *J Thromb Haemost* **17**, 1229-1239, doi:10.1111/jth.14487 (2019).
5 Mann, K. G., Nesheim, M. E., Church, W. R., Haley, P. & Krishnaswamy, S. Surface-dependent reactions of the vitamin K-dependent enzyme complexes. *Blood* **76**, 1-16 (1990).
6 Broad, A. J., Sutherland, S. K. & Coulter, A. R. The lethality in mice of dangerous Australian and other snake venom. *Toxicon* **17**, 661-664, doi:10.1016/0041-0101(79)90245-9 (1979).
7 Masci, P. P., Whitaker, A. N. & de Jersey, J. Purification and characterization of a prothrombin activator from the venom of the Australian brown snake, Pseudonaja textilis textilis. *Biochem Int* **17**, 825-835 (1988).
8 Speijer, H., Govers-Riemslag, J. W., Zwaal, R. F. & Rosing, J. Prothrombin activation by an activator from the venom of Oxyuranus scutellatus (Taipan snake). *J Biol Chem* **261**, 13258-13267 (1986).
9 Walker, F. J., Owen, W. G. & Esmon, C. T. Characterization of the prothrombin activator from the venom of Oxyuranus scutellatus scutellatus (taipan venom). *Biochemistry* **19**, 1020-1023, doi:10.1021/bi00546a029 (1980).
10 St Pierre, L. *et al.* Comparative analysis of prothrombin activators from the venom of Australian elapids. *Mol Biol Evol* **22**, 1853-1864, doi:10.1093/molbev/msi181 (2005).
11 Rao, V. S., Swarup, S. & Kini, R. M. The nonenzymatic subunit of pseutarin C, a prothrombin activator from eastern brown snake (Pseudonaja textilis) venom, shows structural similarity to mammalian coagulation factor V. *Blood* **102**, 1347-1354, doi:10.1182/blood-2002-12-3839 (2003).
12 Rao, V. S., Swarup, S. & Manjunatha Kini, R. The catalytic subunit of pseutarin C, a group C prothrombin activator from the venom of Pseudonaja textilis, is structurally similar to mammalian blood coagulation factor Xa. *Thrombosis and haemostasis* **92**, 509-521, doi:10.1160/TH04-03-0144 (2004).
13 Rao, V. S. & Kini, R. M. Pseutarin C, a prothrombin activator from Pseudonaja textilis venom: its structural and functional similarity to mammalian coagulation factor Xa-Va complex. *Thrombosis and haemostasis* **88**, 611-619 (2002).
14 Bos, M. H. *et al.* Venom factor V from the common brown snake escapes hemostatic regulation through procoagulant adaptations. *Blood* **114**, 686-692, doi:10.1182/blood-2009-02-202663 (2009).
15 Bos, M. H. & Camire, R. M. Procoagulant adaptation of a blood coagulation prothrombinase-like enzyme complex in australian elapid venom. *Toxins (Basel)* **2**, 1554-1567, doi:10.3390/toxins2061554 (2010).
16 Lechtenberg, B. C. *et al.* Crystal structure of the prothrombinase complex from the venom of Pseudonaja textilis. *Blood* **122**, 2777-2783, doi:10.1182/blood-2013-06-511733 (2013).
17 Schreuder, M. *et al.* Evolutionary Adaptations in Pseudonaja Textilis Venom Factor X Induce Zymogen Activity and Resistance to the Intrinsic Tenase Complex. *Thrombosis and haemostasis* **120**, 1512-1523, doi:10.1055/s-0040-1715441 (2020).

18 Verhoef, D. *et al.* Functional implications of the unique disulfide bond in venom factor V from the Australian common brown snake Pseudonaja textilis. *Toxin Reviews* **33**, 37-41, doi:10.3109/15569543.2013.844712 (2014).
19 Egan, J. O., Kalafatis, M. & Mann, K. G. The effect of Arg306-->Ala and Arg506-->Gln substitutions in the inactivation of recombinant human factor Va by activated protein C and protein S. *Protein Sci* **6**, 2016-2027, doi:10.1002/pro.5560060922 (1997).
20 Dahlback, B. & Villoutreix, B. O. The anticoagulant protein C pathway. *FEBS Lett* **579**, 3310-3316, doi:10.1016/j.febslet.2005.03.001 (2005).
21 Kalafatis, M., Rand, M. D. & Mann, K. G. The mechanism of inactivation of human factor V and human factor Va by activated protein C. *J Biol Chem* **269**, 31869-31880 (1994).
22 Kalafatis, M. & Mann, K. G. Role of the membrane in the inactivation of factor Va by activated protein C. *J Biol Chem* **268**, 27246-27257 (1993).
23 Nicolaes, G. A. *et al.* Peptide bond cleavages and loss of functional activity during inactivation of factor Va and factor VaR506Q by activated protein C. *J Biol Chem* **270**, 21158-21166, doi:10.1074/jbc.270.36.21158 (1995).
24 Mann, K. G., Hockin, M. F., Begin, K. J. & Kalafatis, M. Activated protein C cleavage of factor Va leads to dissociation of the A2 domain. *J Biol Chem* **272**, 20678-20683 (1997).
25 Higgins, D. L. & Mann, K. G. The interaction of bovine factor V and factor V-derived peptides with phospholipid vesicles. *J Biol Chem* **258**, 6503-6508 (1983).
26 Toso, R. & Camire, R. M. Removal of B-domain sequences from factor V rather than specific proteolysis underlies the mechanism by which cofactor function is realized. *J Biol Chem* **279**, 21643-21650, doi:10.1074/jbc.M402107200 (2004).
27 Krishnaswamy, S. & Walker, R. K. Contribution of the prothrombin fragment 2 domain to the function of factor Va in the prothrombinase complex. *Biochemistry* **36**, 3319-3330, doi:10.1021/bi9623993 (1997).
28 Verhoef, D. *et al.* Engineered factor Xa variants retain procoagulant activity independent of direct factor Xa inhibitors. *Nat Commun* **8**, 528, doi:10.1038/s41467-017-00647-9 (2017).
29 van der Neut Kolfschoten, M. *et al.* Factor Va is inactivated by activated protein C in the absence of cleavage sites at Arg-306, Arg-506, and Arg-679. *J Biol Chem* **279**, 6567-6575, doi:10.1074/jbc.M308574200 (2004).
30 Rapaport, D. C. The Art of Molecular Dynamics Simulation. *J. Chem. Educ.* **76**, 171 (1999).
31 Shim, J. Y., Lee, C. J., Wu, S. & Pedersen, L. G. A model for the unique role of factor Va A2 domain extension in the human ternary thrombin-generating complex. *Biophysical chemistry* **199**, 46-50, doi:10.1016/j.bpc.2015.02.003 (2015).
32 Krieger, E. & Vriend, G. YASARA View - molecular graphics for all devices - from smartphones to workstations. *Bioinformatics* **30**, 2981-2982, doi:10.1093/bioinformatics/btu426 (2014).
33 Maier, J. A. *et al.* ff14SB: Improving the Accuracy of Protein Side Chain and Backbone Parameters from ff99SB. *J Chem Theory Comput* **11**, 3696-3713, doi:10.1021/acs.jctc.5b00255 (2015).
34 Ryckaert, J., Ciccotti, G. & Berendsen, H. J. C. Numerical integration of the cartesian equations of motion of a system with constraints: molecular dynamics of n-alkanes. *J. Chem. Theory Comput.* **23**, 327–341 (1977).
35 Case, D. A. *et al.* AMBER 2016. *University of California, San Francisco* (2016).
36 Genheden, S. & Ryde, U. The MM/PBSA and MM/GBSA methods to estimate ligand-binding affinities. *Expert Opin Drug Discov* **10**, 449-461, doi:10.1517/17460441.2015.1032936 (2015).
37 Norstrom, E., Thorelli, E. & Dahlback, B. Functional characterization of recombinant FV Hong Kong and FV Cambridge. *Blood* **100**, 524-530, doi:10.1182/blood-2002-02-0343 (2002).
38 Rosing, J. *et al.* Effects of protein S and factor Xa on peptide bond cleavages during inactivation of factor Va and factor VaR506Q by activated protein C. *J Biol Chem* **270**, 27852-27858 (1995).

39 Walker, F. J. Regulation of activated protein C by a new protein. A possible function for bovine protein S. *J Biol Chem* **255**, 5521-5524 (1980).
40 Nicolaes, G. A., Villoutreix, B. O. & Dahlback, B. Partial glycosylation of Asn2181 in human factor V as a cause of molecular and functional heterogeneity. Modulation of glycosylation efficiency by mutagenesis of the consensus sequence for N-linked glycosylation. *Biochemistry* **38**, 13584-13591, doi:10.1021/bi991165r (1999).
41 Minh Le, T. N., Reza, M. A., Swarup, S. & Kini, R. M. Gene duplication of coagulation factor V and origin of venom prothrombin activator in Pseudonaja textilis snake. *Thrombosis and haemostasis* **93**, 420-429, doi:10.1160/TH04-11-0707 (2005).
42 Jiang, Y. & Doolittle, R. F. The evolution of vertebrate blood coagulation as viewed from a comparison of puffer fish and sea squirt genomes. *Proc Natl Acad Sci U S A* **100**, 7527-7532, doi:10.1073/pnas.0932632100 (2003).
43 Ponczek, M. B., Gailani, D. & Doolittle, R. F. Evolution of the contact phase of vertebrate blood coagulation. *J Thromb Haemost* **6**, 1876-1883, doi:10.1111/j.1538-7836.2008.03143.x (2008).
44 Doolittle, R. F. & Feng, D. F. Reconstructing the evolution of vertebrate blood coagulation from a consideration of the amino acid sequences of clotting proteins. *Cold Spring Harb Symp Quant Biol* **52**, 869-874 (1987).
45 Davidson, C. J., Tuddenham, E. G. & McVey, J. H. 450 million years of hemostasis. *J Thromb Haemost* **1**, 1487-1494 (2003).
46 Joseph, J. S., Chung, M. C., Mirtschin, P. J. & Kini, R. M. Effect of snake venom procoagulants on snake plasma: implications for the coagulation cascade of snakes. *Toxicon* **40**, 175-183 (2002).
47 Omar, M. N. & Mann, K. G. Inactivation of factor Va by plasmin. *J Biol Chem* **262**, 9750-9755 (1987).
48 Kalafatis, M. & Mann, K. G. The role of the membrane in the inactivation of factor va by plasmin. Amino acid region 307-348 of factor V plays a critical role in factor Va cofactor function. *J Biol Chem* **276**, 18614-18623, doi:10.1074/jbc.M007134200 (2001).
49 Cederholm-Williams, S. A. Concentration of plasminogen and antiplasmin in plasma and serum. *J Clin Pathol* **34**, 979-981, doi:10.1136/jcp.34.9.979 (1981).
50 Reza, M. A., Minh Le, T. N., Swarup, S. & Manjunatha Kini, R. Molecular evolution caught in action: gene duplication and evolution of molecular isoforms of prothrombin activators in Pseudonaja textilis (brown snake). *J Thromb Haemost* **4**, 1346-1353, doi:10.1111/j.1538-7836.2006.01969.x (2006).
51 Kalafatis, M. & Mann, K. G. Factor V: Dr. Jeckyll and Mr. Hyde. *Blood* **101**, 20-30 (2003).
52 Majumder, R., Quinn-Allen, M. A., Kane, W. H. & Lentz, B. R. A phosphatidylserine binding site in factor Va C1 domain regulates both assembly and activity of the prothrombinase complex. *Blood* **112**, 2795-2802, doi:10.1182/blood-2008-02-138941 (2008).
53 Qureshi, S. H., Yang, L., Manithody, C. & Rezaie, A. R. Membrane-dependent interaction of factor Xa and prothrombin with factor Va in the prothrombinase complex. *Biochemistry* **48**, 5034-5041, doi:10.1021/bi900240g (2009).
54 Dirven, R. J., Vos, H. L. & Bertina, R. M. The R306G and R506Q mutations in coagulation Factor V reveals additional cleavage sites for Activated Protein C in the R313-R321 region and at R505. *Thromb Res* **125**, 444-450, doi:10.1016/j.thromres.2009.12.005 (2010).
55 Shen, L. & Dahlback, B. Factor V and protein S as synergistic cofactors to activated protein C in degradation of factor VIIIa. *J Biol Chem* **269**, 18735-18738 (1994).
56 Wilhelm, A. R. *et al.* Activated Protein C has a Regulatory Role in Factor VIII Function. *Blood* **137**, 2532-2543, doi:10.1182/blood.2020007562 (2021).
57 Thorelli, E., Kaufman, R. J. & Dahlback, B. Cleavage of factor V at Arg 506 by activated protein C and the expression of anticoagulant activity of factor V. *Blood* **93**, 2552-2558 (1999).
58 Castoldi, E. *et al.* Impaired APC cofactor activity of factor V plays a major role in the APC resistance associated with the factor V Leiden (R506Q) and R2 (H1299R) mutations. *Blood* **103**, 4173-4179, doi:10.1182/blood-2003-10-3578 (2004).